Nanotechnology Perceptions
ISSN 1660-6795
www.nano-ntp.com

Study on Effect of Cations Addition to Mg-Zn Ferrite Nanoparticles: Synthesis and Characterisation

Vinaya[1], Rajani M. R[2], Ravishankar. R[3]

[1]Senior Grade Lecturer, Chemical Engineering Dept., S J Government Polytechnic, Bangalore-560001, Karnataka, India.
[2]Assistant professor, Department of Chemical Engineering, DSCE Bangalore-560111, Karnataka, India.
[3]Head & Professor, Department of Chemical Engineering, DSCE Bangalore-560111, Karnataka, India.

The spinel ferrite nanoparticles have gained huge interest in several technological applications. Synthesis methods and the components of ferrites paly vital role in their features and the present work focus on the same. Various cations such as Bi, Ba, Ag and Cu substituted magnesium ferrites were synthesised using simple solution combustion method. The ferrites were characterised using XRD, FESEM and FTIR for their structure as well as morphology. The morpholocial changes were significant with the variation of cations such as Ba, Ag, Bi and Ca. The one with bismuth interestingly showed flake like morphology and other have showed the mixed morphology. Ferrites with Bi and Ba exhibited greater size than the ones with Ag and Ca. The study aims for the comparison on the varied features of ferrites upon cation variation.

Keywords: Magnesium Zinc ferrites, substitution of cations, flake-like, nanoparticles.

1. Introduction

Magnesium ferrites have gained researchers interests due to their fascinating structural as well as magnetic properties. Their applications are vast in ferrofluids precursors, magnetic storage, contrast amplifying agent in magnetic resonance imaging, in drug delivery and as magnetic refrigerant compounds [1, 2]. These are also used in choke coils, recording heads, noise filters and transformers. Manganese ferrites fall under spinel ferrites [3, 4]. The bulk structure of these spinel, possess an equilibrium distribution of cations, which depend on the several factors such as ionic charges, ionic radii, lattice and crystal field stabilization energy. Ferrites are traditionally synthesized by ceramic process which include solid state reaction with greater

temperature [5-7]. The ferrites acquired from this method suffers a larger and non-uniform sizes which eventually lead to voids formation in the compacts. Such issues could be overcome by opting for other chemical synthesis procedure like hydrothermal, co-precipitation, combustion and air oxidation. These have resulted in ultrafine, homogenous, and pure with narrow distribution of size.

Combustion is one of the simplest synthesis procedure, versatile and swift method of nanomaterial synthesis. Minimum time consumption and lesser energy requirements are the positive features of this procedure. Several nanomaterials such as ZnO, CuO, Fe_2O_3, MoS_2, Fe_3O_4 and many have been synthesized with interesting features. In present work, combustion process is employed for the mixed ferrites synthesis. Mixed ferrites are important, as they are composed of multiple phases of the magnets. Especially, non-magnetic cations are habitually presented into the spinel to increase the magnetic properties [8]. Magnesium-Zinc (Mg Zn) ferrites with the formula $Mg_{1-x}Zn_xFe_2O_4$ are technically important with greater initial permeability. Tsay et al obtained such ferrites with x value varying from 0.4 to 0.7 via hydrothermal method [9]. Hu et. al., have also synthesized Zan-Mg-Fe core-shell microspheres by solvothermal method [10]. Choodamani et al synthesized $Mg_{1-x}Zn_xFe_2O_4$ (x = 0.00…1.00, step 0.25) with a crystallite size varying from 47 to 80 nm via solution combustion method trailed by sintering [11]. Reyes et al have synthesised the same with sol-gel method and obtained quasispherical morphology [12]. Mg Zn ferrites are highly stable and could be regenerated and reused for many cycles in wastewater treatment [13]. Mg Zn ferrites exhibits greater resistivity (10^6 -10^7 Ω cm^{-1}) than that of Mn-Zn (~10^7 Ω cm^{-1}) and is much effective at greater frequencies [14].

Above mentioned core-shell systems have been summoned to suffer reduced magnetization and hence redistribution of cations in the spinel and the presence of surface spines would solve the issue. Distribution of cations among the octahedral (B) and tetrahedral (A) sites of crystal lattice influence the lattice structure of ferrites. Nevertheless, the protagonist of cations vis-à-vis their habitation of B sites instead of A sites is still not clear in deciding the magnetic properties of ferrites. With this context, the present work explore the morphological and structural changes exerted by the distribution of cations in the Mg-Zn ferrite system. Two cations from s block elements (Ca^{2+} and Ba^{2+}), a cation from p block elements (Bi^{3+}) and one from d block elements (Ag^{2+}) were selected for the study giving out Ca^{2+} $MgZn_xFe_2O_4$, Ba^{2+} $MgZn_xFe_2O_4$, $Bi^{3+}MgZn_xFe_2O_4$ and Mg^{2+} $MgZn_xFe_2O_4$. A simple and versatile solution combustion method using urea as a fuel. Prepared mixed ferrites were characterized for structural features using X-ray Diffractometer (XRD) and Fourier Transfer Infrared (FTIT) spectra, morphological features by Field Emission Scanning Electron Microscope (FESEM). The variation in the features of prepared mixed ferrites due to the introduction of various cations is compared and analysed.

2. Materials and methods

2.1 Materials

Required chemicals for synthesis such as magnesium nitrate, zinc nitrate, bismuth nitrate, silver nitrate, calcium nitrate, barium nitrate, sodium hydroxide, hydrochloric acid and urea

were of AR grade and procured from Loba Chemie Pvt Ltd. Double Distilled water was used whenever necessary. A simple combustion method was employed for the synthesis process

2.2 Synthesis of mixed ferrites

Magnesium-zinc mixed ferrites were synthesized by the addition of selected cation contributing precursors and urea as fuel. A stoichiometric ratio of magnesium nitrate, zinc nitrate, ferric nitrate, bismuth nitrate/barium nitrate/calcium nitrate/silver nitrate and the urea (reducing agent) were mixed (ratio 1:0.5:0.5:1:1) for 15 minutes. The solutions were kept in the muffle furnace at 500 ºC for about one minute then cooled to room temperature, powdered and calcined at 650 ºC for 2 hours. The respective products are named as M1 (Mg Zn Bi Ferrite), M2 (Mg Zn Ag Ferrite), M3 (Mg Zn Ca Ferrite) and M4 (Mg Zn Ba Ferrite) and will be pronounced same hereafter for the convenience.

2.3 Characterization

The crystal structures and lattice parameters were analysed by X-ray Diffractometer (XRD) with Cu Kα radiation (λ¼1.5404A1) and a Panlytical X'pert Pro. Surface morphology was studied by scanning electron microscope (SEM) model Hitachi S-3400 N and EDX on Thermo Noran System.

3 Results and Discussions

3.1 XRD analysis

The XRD patterns for all the synthesized series of compounds are provided in the figure 1(a)-(d). X-ray diffractograms of all the four compounds showed a spinel structures. Obtained XRD patterns for all the four composites followed a ferrite XRD patterns of Zn and Mg. The peaks are matching with $MgFe_2O_4$ JCPDS No. 17-0464 [15] and the other one $ZnFe_2O_4$ with the JCPDS card number 22-1012 [16]. However, the shifts in the 2θ values are observed from standard Mg Zn ferrite (from literature) due to the replacement of some of the sites by cations such as Bi^{3+}, Ag^{2+}, Ca^{2+} and Ba^{2+}. In case of Mg Zn ferrite system, a steady increase in the lattice parameters are observed due to the replacement of smaller ionic radii Mg^{2+} ions by the greater ionic radii Zn^{2+} ions [17]. These Zn^{2+} ions intensely choose to lodge on the tetrahedral sites. Whereas, Mg^{2+} and Fe^{3+} sites occupy A and B-sites partially [18, 19]. Also, the displacement of Mg ions by Zn ions promote the displacement of Fe^{3+} ions of A site to B site. Nevertheless, the substitution of selected cations for Fe ions, there exhibit the changes in lattice parameters. A major peak with (hkl) values (311) were observed for all the compounds M1, M2, M3 and M4 at 2θ 35.31, 35.479, 35.55 and 35.76 respectively.

For M1, the Bi^{2+} metal peaks are observed at 26.1, 28.3 and 29.7º, which are in agreement with the standard JCPDS Card No. 85-1329 [20], indicating the presence of Bi^{2+} metal ions. Diffractogram of M2 gave an Ag^{2+} peak at 2θ 34.2º and 46.2º matching to (110) and (003) planes, indicating the presence of Ag metal ions in the obtained composite. These peaks are in well agreement with JCPDS No. 42-0874 [21]. Likewise, calcite peaks were notable for M3 at 29.2º [22]. However, for M4, the Ba^{2+} peaks were not remarkable (peaks of (020) and (220)), which were expected due to the inclusion of Ba^{2+} ions [23]. The distribution of Ba^{2+} ions in the composite was less attributing to its larger size with ionic radius 1.35 Å rather than that of

bivalent character.

The d-spacing and crystallite sites were calculated for all the major peaks of all four compounds using equation (1) and (2)

$$d = \frac{\lambda}{2\sin\theta} \qquad \text{..... (1)}$$

$$D = \frac{K\lambda}{\beta\cos\theta} \qquad \text{..... (2)}$$

Where, d is the interplanar distance, D is crystallite size, λ is the wavelength of the X-ray source, θ is Bragg's diffraction angle and β is the full width half maxima (FWHM) of the peaks. The results obtained are summarized in Table 1. The d-spacing of (311) remained almost same for all four samples. However, the variation in the crystallite size (D) values was significant. For M1, M2, M3 and M4 the crystallite size for (311) peak was 0.166 nm, 0.254 nm, 0.33 nm and 0.58 nm respectively. For M1 and M4 the average crystallite size was almost nearby (0.44 and 0.42 nm) and increased to 0.64 nm to M2 and further to 0.72 for M4. The variations in these parameters are attributed to the changes or distortions occurring in the unit cells and lattices due to the substitution of different cations. Despite of the variations, the peaks are intense and sharp indicating the well-crystallinity of single phase structure.

The difference in lattice parameter (a) was examined by calculating the same using equation (3), where hkl are Miller indices of crystal plane. The calculated a values for M1, M2, M3 and M4 are 0.8404, 0.8381, 0.8365 and 0.8317 for the plane (311) were almost nearby indicating no significant change in the lattice constant.

$$a = d\sqrt{h^2 + k^2 + l^2} \qquad \text{.... (3)}$$

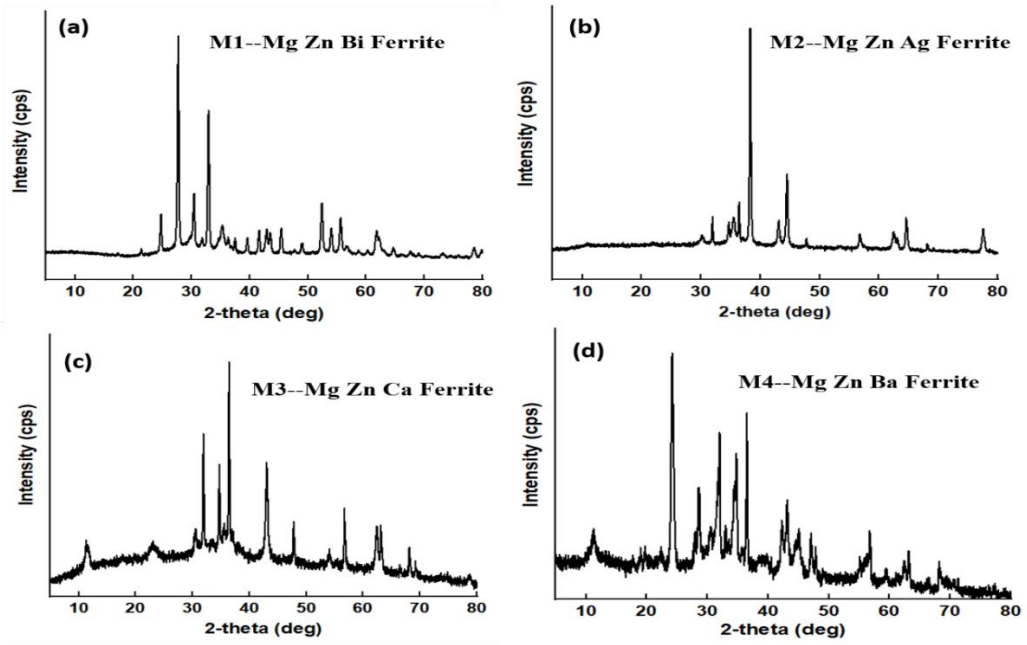

Figure 1: XRD patterns of synthesized mixed ferrites

Table 1: Table summarising the 2θ, d-spacing and crystallite size of the synthesized mixed ferrites.

Mixed ferrite	2-theta(deg)	hkl	d spacing (nm)	D Crystallite size (nm)
M1	17.45	111	0.50760713	0.542425205
	30.401	220	0.29367164	0.480795366
	35.31	311	0.25388682	0.166939792
	37.477	222	0.23968917	0.557892466
	43.503	400	0.20778141	0.454393716
	54.01	422	0.16957803	0.487913427
	58.661	511	0.15719207	0.638636974
	63	440	0.14736883	0.209603133
M2	35.479	311	0.25271608	0.254584116
	38.271	222	0.23489695	0.733140534
	43.03	400	0.20995526	0.457653259
	56.692	511	0.16217527	0.632622973
	63.097	440	0.14716559	0.738550924
	69.2	620	0.13560068	1.034493729
M3	30.46	220	0.293116233	0.312560755
	35.55	311	0.252227603	0.330471472
	36.423	222	0.246379829	0.952459313
	43.027	400	0.209969206	0.374940969
	54.03	422	0.169519978	0.677040112
	56.713	511	0.162120203	1.003038041
	63.132	440	0.147092425	0.862429344
M4	30.46	220	0.293116233	0.365924786
	35.76	311	0.250794375	0.585024982
	36.487	222	0.245962333	0.842107854
	43.169	400	0.20931136	0.325003475
	56.811	511	0.16186378	0.253191172
	63.217	440	0.146915091	0.309047438

3.2 FESEM EDX analysis

Along with structural attributes, the morphology of the mixed ferrites is crucial for the desired applications. The surface morphology for the synthesized ferrites are analysed FESEM and the micrographs are presented in figure 2(a)-2(d). The morphological changes with the variation of substituted cations are dominant and evident from the images. M1 with Bi^{3+} ions substitution showed a flakes like morphology. M2 and M3 showed a spherical morphology

and compound M4 showed a mixed shape which included spherical as well as rod-like shapes. The variation in the grain size, its growth and distribution as well as the morphology depends on the diffusion mechanisms and its coefficients, temperature and even on the composition of dissimilar ions.

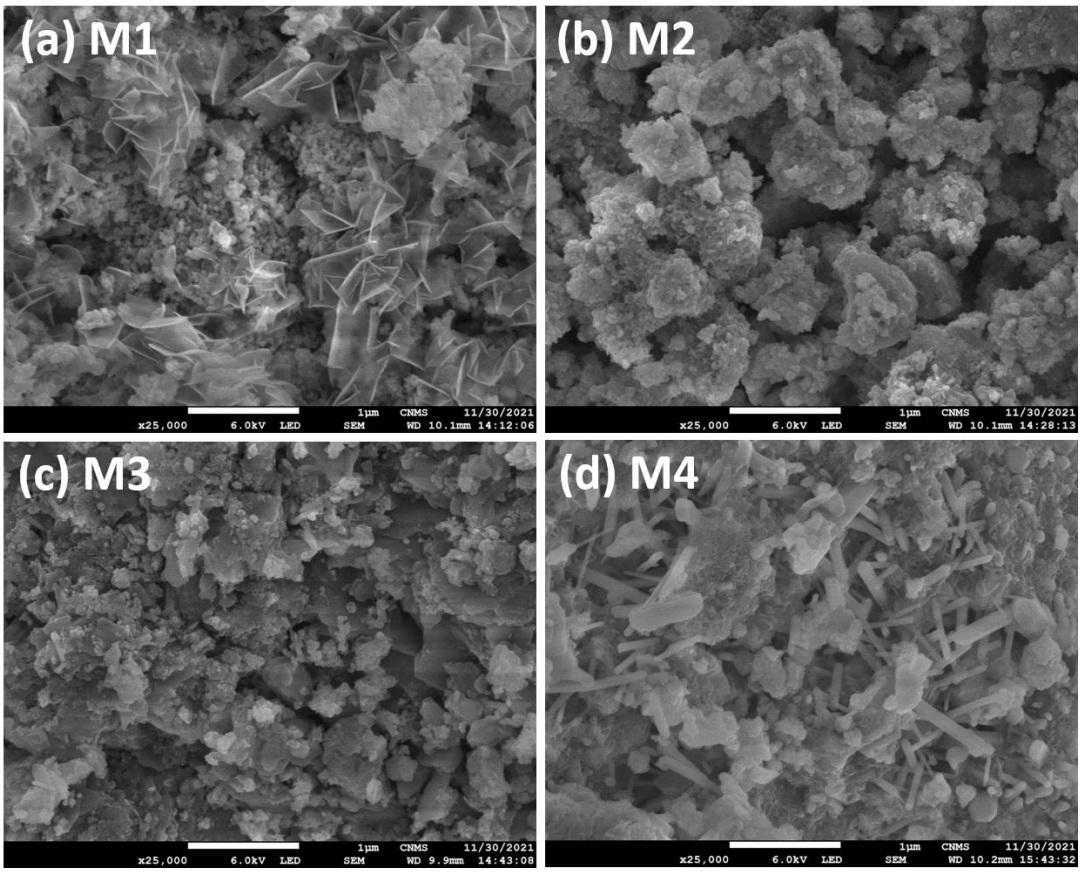

Figure 2: FESEM micrographs of synthesized mixed ferrites

3.3 FT-IR studies

FT-IR adsorption studies is vital as it provides the information on several ordering phenomenon and ions positioning in the crystal along with crystal vibration patterns. The measure IR spectra of mixed ferrites is provided in figure 3. The adsorption bands of mixed ferrites are expected to be in the range of 300 to 800 cm^{-1} [24]. The bands at 450-540 cm^{-1} are assigned to iron-oxygen bonds which are attributed to the iron positioned in tetrahedral and octahedral bands [25]. The molecular water in the molecules gives a peak at 635 cm^{-1}. In all samples, the bands at 572 to 427 cm^{-1} are recognized for tetrahedral and octahedral M-O stretching vibration bands. Where, M can be Fe or Mg. The bands at 1017, 1441, 2920 and 3421 cm^{-1} are assigned for lattice M-O vibrations [26]. The individual FT-IR peaks are presented in supplementary information (SI) for better understanding as Figures SI1 to SI4.

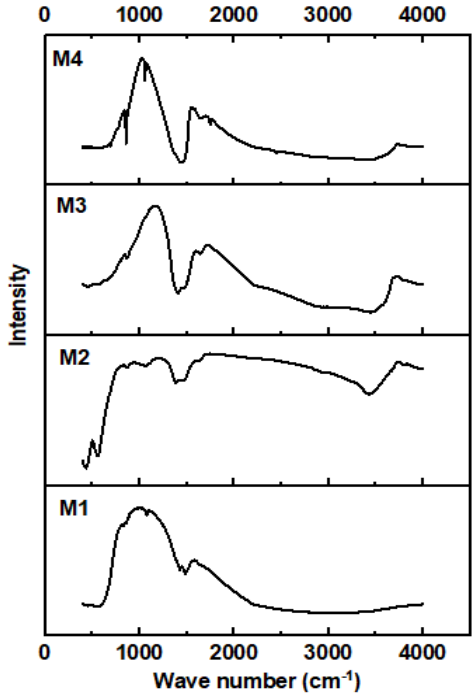

Figure 3: FTIR vibration bands for M1, M2, M3 and M4

More precisely, the two major bands for the samples around 604.3 to 651.3 cm^{-1} (υ_1) and 438.2-452.04 cm^{-1} (υ_2) are attributed to intrinsic vibration of tetrahedral and octahedral Ag-oxygen complexes. The variation in the intensities of these peaks is due to the varied bond length of Fe^{2+}-O^{2-} and $Bi^{2+}/Ag^{2+}/Ca^{2+}/Ba^{2+}$-$O^{2-}$ and mixed cationic distribution [27,28], confirming the spinel structure.

4 Conclusions

Cations such as, Bi, Ag, Ca and Ba substituted magnesium zinc ferrites were synthesized successfully by solution combustion method. The X-ray diffractograms formation of ferrites and the alterations in the 2-theta values with the substitution of cations. The BI substitute ferrite showed a nice flake like morphology, Ba substituted one showed a tod like morphology and other two possessed spherical shapes. The FT-IR spectra also confirm the presence of major peaks pertaining to Mg-Zn ferrites and metal-oxygen stretching vibrations. The paper concludes that; the substation of suitable cations is crucial to attain the required characteristics of ferrites.

Acknowledge

The authors would like to gratefully acknowledge Dayanada Sagar College of Engineering management for the provision of laboratory facility.

References

1. Nigam, A. and S. Pawar, Structural, magnetic, and antimicrobial properties of zinc doped magnesium ferrite for drug delivery applications. Ceramics International, 2020. 46(4): p. 4058-4064.
2. Kaur, N. and M. Kaur, Comparative studies on impact of synthesis methods on structural and magnetic properties of magnesium ferrite nanoparticles. Processing and Application of Ceramics, 2014. 8(3): p. 137-143.
3. Mansour, S. and M. Elkestawy, A comparative study of electric properties of nano-structured and bulk Mn–Mg spinel ferrite. Ceramics International, 2011. 37(4): p. 1175-1180.
4. Amiri, M., M. Salavati-Niasari, and A. Akbari, Magnetic nanocarriers: evolution of spinel ferrites for medical applications. Advances in colloid and interface science, 2019. 265: p. 29-44.
5. Costa, A., et al., Synthesis, microstructure and magnetic properties of Ni–Zn ferrites. Journal of magnetism and magnetic materials, 2003. 256(1-3): p. 174-182.
6. Xia, A., et al., Hexagonal SrFe12O19 ferrites: Hydrothermal synthesis and their sintering properties. Journal of magnetism and magnetic materials, 2013. 332: p. 186-191.
7. Thakur, P., et al., A review on MnZn ferrites: Synthesis, characterization and applications. Ceramics international, 2020. 46(10): p. 15740-15763.
8. Alla, S.K., et al., Mn-substituted cerium oxide nanostructures and their magnetic properties. Materials Research Bulletin, 2018. 104: p. 65-71.
9. Tsay, C.-Y., Y.-C. Chiu, and Y.-K. Tseng, Investigation on structural, magnetic, and FMR properties for hydrothermally-synthesized magnesium-zinc ferrite nanoparticles. Physica B: Condensed Matter, 2019. 570: p. 29-34.
10. Hu, X., et al., Construction of zinc-magnesium-iron multinary spinel core-shell microspheres with enhanced photocatalytic properties of 1, 2-dichlorobenzene toxic species. Journal of Photochemistry and Photobiology A: Chemistry, 2019. 382: p. 111903.
11. Choodamani, C., B. Rudraswamy, and G.T. Chandrappa, Structural, electrical, and magnetic properties of Zn substituted magnesium ferrite. Ceramics International, 2016. 42(9): p. 10565-10571.
12. Reyes-Rodríguez, P.Y., et al., Structural and magnetic properties of Mg-Zn ferrites (Mg1−xZnxFe2O4) prepared by sol-gel method. Journal of Magnetism and Magnetic Materials, 2017. 427: p. 268-271.
13. Tatarchuk, T., et al., Green and ecofriendly materials for the remediation of inorganic and organic pollutants in water. A new generation material graphene: Applications in water technology, 2019: p. 69-110.
14. Yahya, N., et al., Synthesis and charaterization of magnesium zinc ferrites as electromagnetic source. American Journal of Engineering and Applied Sciences, 2008. 1(1): p. 53-56.
15. Wu, X., et al., Electrochemical studies of MgFe2O4@TiO2 core–shell nanospheres as anode material for lithium battery applications. Journal of Materials Science: Materials in Electronics, 2018. 29(20): p. 17872-17880.
16. Naskar, A., H. Khan, and S. Jana, Protein adsorption capability of zinc ferrite nanoparticles formed by a low-temperature solution-based process. Research on Chemical Intermediates, 2017. 43(12): p. 7041-7053.
17. Joshi, G., A. Khot, and S. Sawant, Magnetisation, curie temperature and Y□ K angle studies of Cu substituted and non substituted Ni□ Zn mixed ferrites. Solid state communications, 1988. 65(12): p. 1593-1595.
18. Cheng, J., et al., Synthesis, structural and magnetic properties of epitaxial Mg Fe 2 O 4 thin films by molecular beam epitaxy. Journal of Vacuum Science & Technology B: Microelectronics and Nanometer Structures Processing, Measurement, and Phenomena, 2009. 27(1): p. 148-151.
19. Jotania, R., R. Upadhyay, and R. Kulkarni, Magnetic ordering in Zn substituted Co/sub 1.4/Ge/sub 0.4/Fe/sub 1.2/O/sub 4/spinel system. IEEE transactions on magnetics, 1992. 28(4):

p. 1889-1894.
20. Feng, C., et al., The enhanced photocatalytic properties of BiOCl/BiVO 4 p–n heterojunctions via plasmon resonance of metal Bi. RSC Advances, 2015. 5(93): p. 75947-75952.
21. Elaiyappillai, E., et al., Sonochemically recovered silver oxide nanoparticles from the wastewater of photo film processing units as an electrode material for supercapacitor and sensing of 2, 4, 6-trichlorophenol in agricultural soil samples. Ultrasonics sonochemistry, 2019. 50: p. 255-264.
22. Lee, S.-H., et al. Calcium Ion Extraction from Blast Furnace Slags for the Synthesis of Pure Calcium Carbonate Polymorphs by Accelerated Carbonation. in 5th Asian Particle Technology Symposium, Singapore. 2012.
23. Dimowa, L., et al., Powder XRD Structural Study of Ba2+ Modified Clinoptilolite at Different Stages of the Ion Exchange Process Conducted at Two Temperature Regimes—Room Temperature and 90° C. Minerals, 2020. 10(11): p. 938.
24. Melagiriyappa, E. and H. Jayanna, Structural and magnetic susceptibility studies of samarium substituted magnesium–zinc ferrites. Journal of alloys and compounds, 2009. 482(1-2): p. 147-150.
25. Sharma, R., et al., Improvement in magnetic behaviour of cobalt doped magnesium zinc nano-ferrites via co-precipitation route. Journal of alloys and compounds, 2016. 684: p. 569-581.
26. Pendyala, S.K., et al., Investigations on physical properties of Mg ferrite nanoparticles for microwave applications. Journal of Microwave Power and Electromagnetic Energy, 2019. 53(1): p. 3-11.
27. Jasrotia, R., et al., Synthesis and characterization of Mg-Ag-Mn nano-ferrites for electromagnet applications. Physica B: Condensed Matter, 2019. 569: p. 1-7.
28. Rajani M , R., et al., Carbonaceous MnFe2O4 Nano adsorbent: Synthesis, characterisation and investigations on chromium (VI) ions removal efficiency from aqueous solution. Applied Surface Science Advances, 2023. 16